

# Strong and Weak Chaos in Networks of Semiconductor Lasers with Time-delayed Couplings

Sven Heiligenthal,<sup>1,\*</sup> Thomas Jüngling,<sup>1</sup> Otti D’Huys,<sup>1</sup> Diana A. Arroyo-Almanza,<sup>2,†</sup>  
Miguel C. Soriano,<sup>2</sup> Ingo Fischer,<sup>2</sup> Ido Kanter,<sup>3</sup> and Wolfgang Kinzel<sup>1</sup>

<sup>1</sup>*Institute of Theoretical Physics, University of Würzburg, 97074 Würzburg, Germany*

<sup>2</sup>*Instituto de Física Interdisciplinar y Sistemas Complejos, IFISC (UIB-CSIC),  
Campus Universitat de les Illes Balears, 07122 Palma de Mallorca, Spain*

<sup>3</sup>*Department of Physics, Bar-Ilan University, 52900 Ramat-Gan, Israel*

(Dated: June 5, 2022)

Nonlinear networks with time-delayed couplings may show strong and weak chaos, depending on the scaling of their Lyapunov exponent with the delay time. We study strong and weak chaos for semiconductor lasers, either with time-delayed self-feedback or for small networks. We examine the dependence on the pump current and consider the question whether strong and weak chaos can be identified from the shape of the intensity trace, the auto-correlations and the external cavity modes. The concept of the sub-Lyapunov exponent  $\lambda_0$  is generalized to the case of two time-scale separated delays in the system. We give the first experimental evidence of strong and weak chaos in a network of lasers which supports the sequence ‘weak to strong to weak chaos’ upon monotonically increasing the coupling strength. Finally, we discuss strong and weak chaos for networks with several distinct sub-Lyapunov exponents and comment on the dependence of the sub-Lyapunov exponent on the number of a laser’s inputs in a network.

PACS numbers: 05.45.Xt, 89.75.-k, 02.30.Ks

## I. INTRODUCTION

The cooperative behavior of a system of interacting units is of fundamental interest in nonlinear dynamics. Such complex networks have a wide range of interdisciplinary applications ranging from neural networks to coupled lasers [1–5]. Typically, these units interact by transmitting information about their state to their partners, and in many systems the transmission time is larger than the time scales of the individual units. For this reason, networks with time-delayed couplings are a focus of active research [6, 7].

Time-delayed feedback can produce dynamical instabilities which may lead to deterministic chaos [8–10]. Even a scalar nonlinear differential equation with time-delayed feedback has an infinite-dimensional phase space which favors chaotic solutions. As an example, a single semiconductor laser often exhibits chaotic emission dynamics when its laser beam is reflected back into its cavity by an external mirror. Networks of nonlinear units may, similarly, become chaotic due to time-delayed coupling of the nodes [11].

For networks of identical units, chaos synchronization is possible. Even if the delay times are very long, the units may synchronize onto a common chaotic trajectory without time shift (zero-lag synchronization) [12–14]. Other kinds of synchronization are possible as well, like phase, achronal, anticipated and generalized synchronization. Chaos synchronization is being discussed in the context of secure communication [15, 16].

Recently, two different kinds of chaos have been identified for chaotic networks of time-continuous systems with time-delayed couplings: strong and weak chaos [17]. In the limit of large delay times, the maximal Lyapunov exponent (LE) of the network saturates at a nonzero value for strong chaos, whereas it scales with the inverse delay time for weak chaos. A similar phenomenon has been reported in [9] for time-discrete maps with delay. Only networks exhibiting weak chaos can synchronize to a common chaotic trajectory.

In this paper we extend these investigations on strong and weak chaos focusing on the dynamics of semiconductor lasers. In Sec. II we define the model and the linearized equations which determine the Lyapunov exponents. In Sec. III a single unit with time-delayed feedback is considered. An artificial sub-LE is defined which determines, whether the unit is in the strong or weak chaos phase. The scaling argument of [17] is extended to derive the behavior of the maximal LE in the limit of large delay time. This system is investigated in Sec. IV for semiconductor lasers. Numerical simulations of the Lang-Kobayashi equations yield the transition from weak to strong chaos and back to weak chaos upon monotonically increasing the coupling strength. The scaling just at the transition is derived. Auto-correlations, spatial representations of the chaotic intensity and external cavity modes are calculated to investigate whether one can deduce the type of chaos from a single trajectory. In Sec. V networks of semiconductor lasers are considered. The stability of the synchronization manifold is related to the eigenvalue gap of the coupling matrix and the master stability function. The first experiment on semiconductor lasers which supports the sequence ‘weak to strong to weak chaos’ with increasing coupling strength is demonstrated. Finally, networks with several distinct sub-LEs

\* sven.heiligenthal@physik.uni-wuerzburg.de

† Also with Centro de Investigaciones en Óptica, León 37150, Guanajuato, México.

and certain network patterns are investigated.

## II. THE LANG-KOBAYASHI EQUATIONS AND THEIR LYAPUNOV EXPONENTS

We study the dynamics of coupled semiconductor lasers by means of numerical simulations, complemented by experiments. To this end we use the Lang-Kobayashi (LK) model, which compresses the complex physical processes of a laser in rate equations for only three classical degrees of freedom, namely the complex electric field  $\mathcal{E}(t)$  and the normalized deviation of the charge carrier density  $n(t)$  with respect to the density at the lasing threshold. The rate equations for a single laser without self-feedback read

$$\begin{aligned}\dot{\mathcal{E}}(t) &= \frac{1+i\alpha}{2} G_N n(t) \mathcal{E}(t) \\ n(t) &= (p-1) J_{\text{th}} - \gamma n(t) - [\Gamma + G_N n(t)] |\mathcal{E}(t)|^2\end{aligned}\quad (1)$$

A table of the parameters involved can be found in the appendix. Note that the phase of the electric field  $\phi_e(t) = \arg \mathcal{E}(t)$  in the model is defined to describe only the deviation from  $\omega_0 t$ , which contains the high oscillation frequency of the actual laser mode. Moreover, we have omitted intensity dependent nonlinear gain reduction, which would be taken into account via an additional factor  $(1 + \varepsilon |\mathcal{E}|^2)^{-1}$  with  $\varepsilon \sim 10^{-7}$  for  $G_N$ . All results presented in this paper, which are obtained with the simplified Eq. (1), coincide qualitatively with the results of the complete rate equations. The LEs are calculated by linearizing Eq. (1). The linearization reads

$$\begin{aligned}\delta\dot{\mathcal{E}}(t) &= \frac{1+i\alpha}{2} G_N [n(t) \delta\mathcal{E}(t) + \mathcal{E}(t) \delta n(t)] \\ \delta\dot{n}(t) &= -(\gamma + G_N |\mathcal{E}(t)|^2) \delta n(t) \\ &\quad - 2[\Gamma + G_N n(t)] \Re\{\mathcal{E}^*(t) \delta\mathcal{E}(t)\}.\end{aligned}\quad (2)$$

We describe the system's state by the state vector  $\mathbf{x} = (x_1, x_2, x_3)^\top$  with  $x_1 \equiv \Re\{\mathcal{E}\}$ ,  $x_2 \equiv \Im\{\mathcal{E}\}$ , and  $x_3 \equiv n$ . Consequently, Eq. (1) reads  $\dot{\mathbf{x}} = \mathbf{F}(\mathbf{x})$  and the linearization accordingly  $\delta\dot{\mathbf{x}} = D\mathbf{F}(\mathbf{x}) \delta\mathbf{x}$ . In this notation we introduce time-delayed feedback on a single laser by

$$\dot{\mathbf{x}} = \mathbf{F}(\mathbf{x}) + \sigma \mathbf{H}(\mathbf{x}_\tau), \quad (3)$$

where  $\mathbf{H}(\mathbf{x}) = \exp(-i\omega_0 \tau)(x_1, x_2, 0)^\top$  describes linear coupling by reinjection of laser light into the cavity. The carrier density is not directly affected by the coupling. The coupling rate  $\sigma$  denotes the feedback strength and depends on the reflectivity of the distant mirror as well as absorbers in the light path. The exponential term is a remainder of the transformation from optical phase to relative phase. The linearization of the laser equation with delayed feedback reads

$$\delta\dot{\mathbf{x}} = D\mathbf{F}(\mathbf{x}) \delta\mathbf{x} + \sigma D\mathbf{H}(\mathbf{x}_\tau) \delta\mathbf{x}_\tau \quad (4)$$

and can be used to calculate LEs for a given trajectory  $\mathbf{x}(t)$ , which is obtained by integration of Eq. (3). The

maximal LE  $\lambda_m$  is defined by

$$\lambda_m = \lim_{t \rightarrow \infty} \frac{1}{t} \ln \left\{ \frac{\|\delta\mathbf{x}(t)\|}{\|\delta\mathbf{x}(t_0)\|} \right\} \quad (5)$$

The norm  $\|\mathbf{a}\|$  in our case is  $\sqrt{a_1^2 + a_2^2}$ , meaning that we use only the electric field components of the Lyapunov trajectory  $\delta\mathbf{x}(t)$ . The choice of the norm does not influence the final result, but may have strong influence on the required length of the trajectory to calculate an exponent with sufficiently high accuracy.

Since the system under investigation is a delay system, we formally obtain infinitely many LEs depending on the initial conditions of the linear system. In practice, for random initial conditions after some transient time, the system relaxes onto the most unstable mode revealing the maximal exponent. In the following, we concentrate on the description and prediction of the dependence of  $\lambda_m$  on the feedback parameter  $\sigma$ .

## III. STRONG AND WEAK CHAOS

### A. The sub-Lyapunov exponent and its experimental measurement

Conditional LEs play an important role for synchronization in networks of coupled dynamical systems. More general, when a large system can be divided into two subsystems forming a drive-response scheme (driver:  $\mathcal{D}$ , response:  $\mathcal{R}$ ), it makes sense to define a conditional LE  $\lambda_{\mathcal{R}}$  of the driven system  $\mathcal{R}$  in order to classify the dynamics or to predict synchronization properties [18]. The conditional exponent is often referred to as ‘sub-Lyapunov exponent’ to stress the fact, that it characterizes a subsystem. If the sub-exponent is negative,  $\mathcal{R}$  is in a state of generalized synchronization with  $\mathcal{D}$ . Otherwise  $\mathcal{R}$  is autonomously chaotic, meaning that its state is not determined by the state of  $\mathcal{D}$ .

The sign of a sub-LE can be measured experimentally. To this end a copy  $\mathcal{R}'$  of  $\mathcal{R}$  has to be created.  $\mathcal{R}'$  is then coupled to  $\mathcal{D}$  in the same way that  $\mathcal{R}$  is, meaning both units receive the same driving signal. If  $\lambda_{\mathcal{R}} < 0$ , then  $\mathcal{R}'$  and  $\mathcal{R}$  synchronize completely, otherwise not. This procedure is known as the Abarbanel test [19] for generalized synchronization between  $\mathcal{D}$  and  $\mathcal{R}$ .

A similar situation is present in case of a system with time-delayed feedback. Although quite against intuition, one can imagine partitioning of the delay system into non-delayed dynamical unit  $\mathcal{A} \cong \mathcal{R}$  and transmission line  $\mathcal{A}_\tau \cong \mathcal{D}$ . The sub-Lyapunov exponent of the unit arises only from the instantaneous part of the equations of motion, and has therefore been referred to as ‘instantaneous Lyapunov exponent’ [17]. However, in this paper we keep the notion ‘sub-Lyapunov exponent’ and denote it as  $\lambda_0$ . Formally, from the equations of motion

$$\dot{\mathbf{x}} = \mathbf{F}(\mathbf{x}) + \sigma \mathbf{H}(\mathbf{x}_\tau) \quad (6)$$

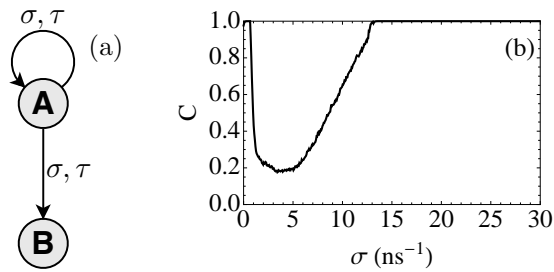


Figure 1. (a) Configuration to measure the difference between strong and weak chaos. (b) Simulated isochronal cross-correlation  $C$  between two lasers coupled according to the setup presented in (a) for a delay time  $\tau = 10$  ns and a pump current  $p = 1.02$  vs coupling strength  $\sigma$ .

we obtain  $\lambda_0$  by integrating the linearization

$$\dot{\delta \mathbf{x}}_0 = DF(\mathbf{x}) \delta \mathbf{x}_0 \quad (7)$$

$$\lambda_0 = \lim_{t \rightarrow \infty} \frac{1}{t} \ln \left\{ \frac{\|\delta \mathbf{x}_0(t)\|}{\|\delta \mathbf{x}_0(t_0)\|} \right\}. \quad (8)$$

Alternatively, we can define  $\lambda_0$  via the evolution operator of Eq. 7

$$\delta \mathbf{x}_0(t) = U(t, t_0) \delta \mathbf{x}_0(t_0), \quad (9)$$

with  $U(t_0, t_0) = \mathbb{1}$ . Then

$$\lambda_0 = \max_i \lim_{t \rightarrow \infty} \frac{1}{2t} \ln(\text{eig}_i \{U^\top(t, t_0) U(t, t_0)\}). \quad (10)$$

It is important to mention, that although the delay term is skipped in the defining equation for  $\lambda_0$ , the delay parameters  $\sigma$  and  $\tau$  enter indirectly via the trajectory  $\mathbf{x}(t)$ , which is inserted in the linearization Eq. (7). As we show later, this dependence is non-negligible and it is possible to change the sign of  $\lambda_0$  only by variation of a delay parameter.

The consequence of the sign of  $\lambda_0$  is documented in recent work [17]. If  $\lambda_0 > 0$ , we call the resulting chaotic dynamics ‘strong chaos’, else if  $\lambda_0 < 0$  but the delay system is still chaotic, we define ‘weak chaos’. The sign of  $\lambda_0$  has two major implications. Firstly, for a single delay system it determines the scaling of the maximal LE with delay time. Secondly, for a network of delay-coupled units it determines the possibility to synchronize the units at large delay times. If the units are strongly chaotic, the delayed coupling cannot compensate for the exponential divergence of two nearby trajectories of any two systems in the network, and therefore synchronization is not possible. On the other hand, for weak chaos, synchronization is in principle possible and depends on the network topology.

In analogy to the general Abarbanel test, we can measure the sign of the sub-LE  $\lambda_0$  using an auxiliary system approach as shown in Fig. 1(a). The system  $\mathcal{B} \hat{=} \mathcal{R}'$  is a copy of the undelayed system  $\mathcal{A} \hat{=} \mathcal{R}$ . In the presented

coupling topology both units are receiving the same signal  $\mathcal{A}_\tau \hat{=} \mathcal{D}$ . If we analyze the equations of motion for this setup in the vicinity of the complete synchronization manifold (SM) of  $\mathcal{A}$  and  $\mathcal{B}$ , we obtain in linear approximation the same system, by which we also have defined  $\lambda_0$ . This means, that in the test setup both units synchronize if and only if they are in weak chaos. Synchronization is unstable if and only if they are in strong chaos. The result of a numerical simulation of this setup for two coupled semiconductor lasers is shown in Fig. 1(b) showing the cross-correlation between  $\mathcal{A}$  and  $\mathcal{B}$  in dependence on the coupling strength  $\sigma$ . A cross-correlation  $C = 1$  corresponds to complete synchronization and implies the presence of weak chaos. The drop-down of the correlation indicates transitions from weak to strong and back to weak chaos by increasing  $\sigma$ . We discuss this behavior in detail in Sec. IV.

## B. Scaling of the maximal Lyapunov exponent with the delay time

As we show in the following, the sub-LE  $\lambda_0$ , as introduced by Eqs. (6)-(8), determines the scaling behavior of the maximal LE  $\lambda_m$ , as introduced by Eqs. (3)-(5), with the delay time. Note that there is always a spectrum of LEs, in this case a countable infinite set.  $\lambda_m$  is the maximal exponent of this spectrum. Further we assume the existence of a single attractor and the ergodicity of the trajectory  $\mathbf{x}(t)$  so that we can also skip the dependence on the initial conditions.

We now distinguish between two cases: a) Strong chaos,  $\lambda_0 > 0$ . b) Weak chaos,  $\lambda_0 < 0$ . In order to derive a scaling relation  $\lambda_m(\tau)$ , we have to assume, that  $\lambda_0(\tau) = \text{const}$ . In a strict sense this is never true, but for sufficiently large  $\tau$  one always observes a saturation effect and a decrease of remaining fluctuations in  $\lambda_0(\tau)$ , so that the assumption of a constant value is valid.

a. *Strong chaos*,  $\lambda_0 > 0$ . We start from the linearization Eq. (4). If  $\lambda_0 > 0$ , for large  $\tau$  the instantaneous term becomes dominant and the delay term becomes negligible. This can be seen from the coordinate transformation

$$\delta \mathbf{x}(t) = e^{\lambda_0 t} \delta \mathbf{z}(t), \quad (11)$$

which results in

$$\dot{\delta \mathbf{z}} = [DF(\mathbf{x}) - \lambda_0 \cdot \mathbb{1}] \delta \mathbf{z} + \sigma e^{-\lambda_0 \tau} DH(\mathbf{x}_\tau) \delta \mathbf{z}_\tau. \quad (12)$$

For large delay times the delay term in this equation becomes exponentially small and can be neglected. The resulting Lyapunov exponent of the transformed system can therefore be estimated as  $\lambda_z \approx 0$ . This implies that in the original coordinates  $\lambda_m \approx \lambda_0$ , meaning that the Lyapunov becomes independent of  $\tau$  for large delays.

b. *Weak chaos*,  $\lambda_0 < 0$ . In this case we can estimate the scaling of the LE by considering a stroboscopic sequence of the evolution of our linear system,  $\delta \mathbf{x}_n(\theta) = \delta \mathbf{x}(\theta + n\tau)$  with  $n \in \mathbb{Z}$  and  $\theta \in ]-\tau, 0]$ . One

can introduce a growth factor (Lyapunov multiplier) by  $\|\delta\mathbf{x}_{n+1}\| = \mu_n \|\delta\mathbf{x}_n\|$ , so that the LE becomes

$$\lambda_m = \lim_{l \rightarrow \infty} \frac{1}{l\tau} \sum_{n=1}^l \ln \mu_n = \frac{1}{\tau} \ln C, \quad (13)$$

where  $C$  is the geometric mean of all multipliers. In the following we show, that for sufficiently large delay times the multipliers  $\mu_n$  do not depend on  $\tau$ , hence the LE is of order  $\tau^{-1}$ , meaning that in weak chaos a perturbation of the chaotic system grows on the timescale of the delay time. To this end, we introduce the variation-of-constants formula, which provides an integral version of our initial delay differential equation (4), and evaluate it at  $\theta = 0$

$$\begin{aligned} \delta\mathbf{x}_{n+1}(0) &= U_n(0, -\tau) \delta\mathbf{x}_n(0) \\ &+ \sigma \int_{-\tau}^0 dt U_n(0, t) DH[\mathbf{x}_n(t)] \delta\mathbf{x}_n(t). \end{aligned} \quad (14)$$

It contains the evolution operator  $U_n(t_2, t_1)$  of the auxiliary system Eq. (7) on the  $n$ -th  $\tau$ -interval. This operator is exponential in  $t_2 - t_1$ , i.e. with respect to a suitable matrix norm it holds that for  $t_2 > t_1$

$$\|U(t_2, t_1)\| < U_0 \exp[\alpha(t_2 - t_1)] \quad (15)$$

with  $\lambda_0 < \alpha < 0$ . The bound provided by  $U_0$  and  $\alpha$  should cover potential bursts typical for the linearization of a chaotic flow. Because of this exponential bound, there is some time  $\tau_0 \propto \alpha^{-1}$ , such that the term with  $U(0, -\tau)$  can be neglected in Eq. (14), if  $\tau > \tau_0$ . Additionally, the integral has only significant contributions in a small range close to the end of the integration interval, namely for  $t \in [-\tau_0, 0]$ . This means that a further increase of  $\tau$  beyond  $\tau_0$  does not affect the integral. Therefore the multiplier introduced above can be estimated by

$$\begin{aligned} \mu_n &= \frac{\sigma}{\|\delta\mathbf{x}_n(0)\|} \left\| \int_{-\tau_0}^0 dt U_n(0, t) DH[\mathbf{x}_n(t)] \delta\mathbf{x}_n(t) \right\| \\ &+ \mathcal{O}(e^{-\alpha\tau}). \end{aligned} \quad (16)$$

In leading order, this expression does not depend on the delay time. It depends on  $\lambda_0$ ,  $\sigma$  and a set  $\mathbf{q}$  of other (yet unknown) statistical properties of the chaotic trajectory. Hence we can write

$$\lambda_m = \frac{1}{\tau} \ln C(\lambda_0, \sigma, \mathbf{q}). \quad (17)$$

For comparison: Given a Floquet problem, in which the driving trajectory is  $\tau$ -periodic ( $\mathbf{x}(t) = \mathbf{x}(t + \tau)$ ) and the coupling is linear and diagonal ( $DH[\mathbf{x}(t)] \equiv \mathbb{1}$ ), we obtain  $C = -\sigma/\lambda_0$ .

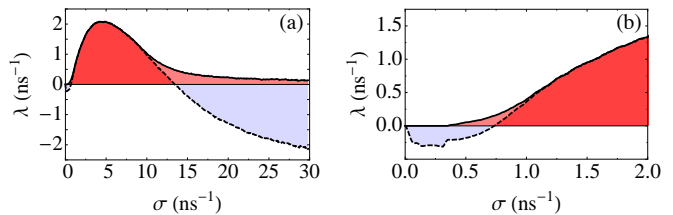


Figure 2. (Color online) (a) Maximal Lyapunov exponent (LE)  $\lambda_m$  (solid line) and sub-LE  $\lambda_0$  (dashed line) of a single laser with self-feedback for a delay time  $\tau = 10$  ns vs coupling strength  $\sigma$ . (b) Enlarged view of left diagram for small coupling strengths  $\sigma$ .

#### IV. SINGLE LASER WITH TIME-DELAYED SELF-FEEDBACK

##### A. Transitions between strong and weak chaos

We now discuss the most simple system which can show strong and weak chaos: a single laser with time-delayed self-feedback. The laser dynamics is modeled by the LK equations. The parameter values can be found in the appendix. If not mentioned differently, all diagrams are made for a delay time of  $\tau = 10$  ns and a pump current of  $p = 1.02$ .

Fig. 2(a) shows the maximal LE  $\lambda_m$  (solid line) and sub-LE  $\lambda_0$  (dashed line) of a single laser with self-feedback in dependence on the coupling strength  $\sigma$ . Although the coupling strength does not enter directly into the conditional equation of the sub-LE, as it would be the case e.g. for a linear damping term with  $\sigma$ , the sign of the sub-LE changes from positive to negative for large coupling strengths only through the different dynamics  $\mathbf{x}(t)$  which is inserted into Eq. (7). Thus, there is a transition from strong to weak chaos with growing  $\sigma$ . In the region of small coupling strengths, Fig. 2(b), however, there is an additional region of weak chaos where the laser is already chaotic, i.e.  $\lambda_m > 0$ , but the sub-LE is still negative. Hence, there is an additional transition from weak to strong chaos upon increasing  $\sigma$  for small coupling strengths.

Overall, we observe a transition from periodic behavior (Goldstone mode with  $\lambda_m = 0$ ) to weak chaos and from there transitions to strong chaos and back to weak chaos upon monotonically increasing the coupling strength.

Fig. 3 shows the different behaviors of the maximal LE and the sub-LE for the regimes of weak, Fig. 3(a), and strong chaos, Fig. 3(b), in dependence on the delay time  $\tau$ . As soon as the delay time is large compared with the internal time scales of the laser, the sub-LE  $\lambda_0$  remains constant with increasing  $\tau$  for both weak and strong chaos. For weak chaos,  $\lambda_m$  decreases like  $1/\tau$  for growing  $\tau$ . For strong chaos,  $\lambda_m$  converges exponentially to the positive sub-LE  $\lambda_0$ .

The product  $\lambda_m \tau$  is the relevant dimensionless quantity describing chaoticity in systems with delay. For

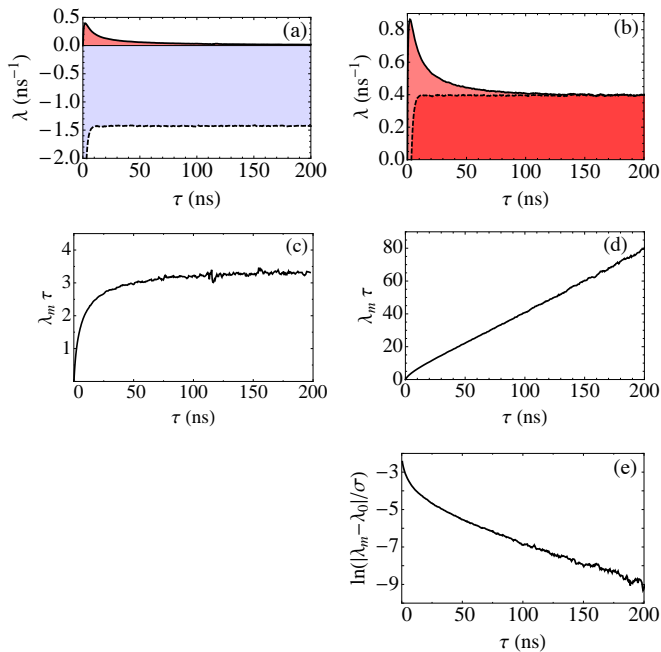


Figure 3. (Color online) Maximal LE  $\lambda_m$  (solid line) and sub-LE  $\lambda_0$  (dashed line) of a single laser with self-feedback for (a) weak chaos ( $\sigma = 21 \text{ ns}^{-1}$ ) and (b) strong chaos ( $\sigma = 12 \text{ ns}^{-1}$ ) vs delay time  $\tau$ . Product  $\lambda_m \tau$  of a single laser with self-feedback for (c) weak chaos ( $\sigma = 21 \text{ ns}^{-1}$ ) and (d) strong chaos ( $\sigma = 12 \text{ ns}^{-1}$ ) vs delay time  $\tau$ . (e)  $\ln(|\lambda_m - \lambda_0|/\sigma)$  of a single laser with self-feedback vs delay time  $\tau$  for strong chaos ( $\sigma = 12 \text{ ns}^{-1}$ ).

weak chaos, this product saturates at a constant value [Fig. 3(c)] which depends on the coupling strength. This dependence is caused by different levels of fluctuations for different  $\sigma$ . Also the delay time  $\tau$  at which the product  $\lambda_m \tau$  has reached the saturation value up to a fixed distance  $\delta$  depends on  $\sigma$ : The closer one is at the critical coupling strength  $\sigma_{\text{crit}}$  where  $\lambda_0 = 0$ , the larger the delay time has to be, i. e. saturation happens later for larger  $\tau$ .

For strong chaos, on the contrary,  $\lambda_m \tau$  grows linearly with increasing  $\tau$  [Fig. 3(d)] since  $\lambda_m$  gets constant as shown in Fig. 3(b). Fig. 3(e) confirms that the convergence  $\lambda_m \rightarrow \lambda_0 > 0$  happens exponentially with  $\tau$ . The characteristic exponent of this convergence, however, is much larger (i. e. the convergence is slower) than one would expect from analytic calculations for a simple model with constant coefficients. This effect is caused by the fluctuations of  $DF[\mathbf{x}(t)]$  which act like multiplicative noise in Eq. (4) and (7) [20].

Fig. 4 shows the special limit case between strong and weak chaos when the sub-LE  $\lambda_0 = 0$  for sufficiently large delay times  $\tau$ . In Fig. 4(a) one can see that the maximal LE still decays with increasing  $\tau$ . However, it does so very slowly. Fig. 4(b) shows the consequence for the product  $\lambda_m \tau$  at the critical point: Neither does it grow linearly with  $\tau$  like for strong chaos, nor does it saturate at a constant value for finite delay times like for weak chaos. The point where the product  $\lambda_m \tau$  saturates is

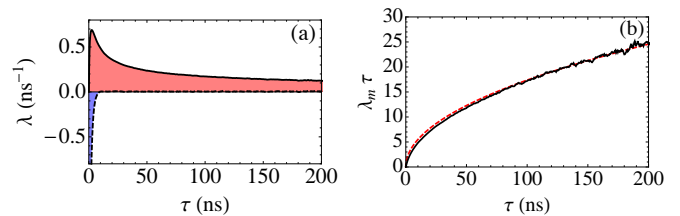


Figure 4. (Color online) (a) Maximal LE  $\lambda_m$  (solid line) and sub-LE  $\lambda_0$  (dashed line) and (b) product  $\lambda_m \tau$  (black solid line) of a single laser with self-feedback in comparison with the least-squares fit of  $\sqrt{\tau}$  (red dashed line) for critical coupling strength where transition between strong and weak chaos occurs ( $\sigma_{\text{crit}} = 13.4 \text{ ns}^{-1}$ ) vs delay time  $\tau$ .

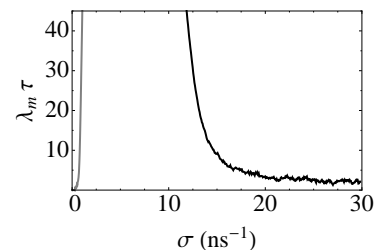


Figure 5. Product  $\lambda_m \tau$  of a single laser with self-feedback vs coupling strength  $\sigma$  for a delay time  $\tau = 100 \text{ ns}$ .

only reached for infinitely large delay times  $\tau \rightarrow \infty$ .  $\lambda_m \tau$  rather grows like  $\sqrt{\tau}$  as is shown by the least-squares fit with  $\sqrt{\tau}$  (red dashed line) in Fig. 4(b). It turns out that this behavior can be explained as well with the effect of the multiplicative fluctuations of  $DF[\mathbf{x}(t)]$ . These fluctuations can be shown to appear in simple systems in which they are modeled as multiplicative white noise [20].

Fig. 5(a) shows that for weak chaos and a very large delay time  $\tau \rightarrow \infty$ , the product  $\lambda_m \tau$  undergoes a phase transition and diverges in the proximity of the critical coupling strengths  $\sigma_{\text{crit},1}$  (gray line) and  $\sigma_{\text{crit},2}$  (black line).

We were able to find the occurrence of strong and weak chaos and the transitions between them by changing the coupling strength  $\sigma$  also for the Rössler and Lorenz dynamics. The Stuart-Landau, FitzHugh-Nagumo and continuous Ikeda dynamics only show weak chaos.

## B. Scaling of the sub-Lyapunov exponent with the laser pump current

We study the dependence of the sub-LE on the laser pump current. Fig. 6(a) shows the sub-LE as a function of the feedback strength  $\sigma$  for different values of the pump current. We find that the curves all follow the same pattern described in the previous section. The sub-LE is negative for small and for large values of the feedback strength. The agreement is even quantitative. We find that the sub-LE and coupling strength scale with the square root of the effective pump current  $\sqrt{p-1}$  above

the lasing threshold. Fig. 6(b) shows the maximum of the sub-LE  $\lambda_{0,\max}$ , the feedback strength  $\sigma_{0,\max}$  for which the sub-LE is maximal, and the critical feedback strength  $\sigma_{0,\text{crit}}$  where  $\lambda_0 = 0$  as a function of the effective pump current  $p - 1$ . The data is shown in a double-logarithmic scale, indicating a slope of  $1/2$ . In Fig. 6(c) the sub-LEs are rescaled with  $\sqrt{p - 1}$ . We find that this scaling relation holds well for small coupling strengths. For larger coupling strengths the sub-LEs diverge for different pump currents.

To explain this scaling behavior we introduce the following rescaling of the laser parameters

$$\begin{aligned} N &= \sqrt{\frac{G_N}{\Gamma N_{\text{sol}}}} \frac{n}{\sqrt{p-1}} \\ E &= \sqrt{\frac{\Gamma}{\gamma N_{\text{sol}}}} \frac{\mathcal{E}}{\sqrt{p-1}} \\ K &= \frac{1}{\sqrt{G_N N_{\text{sol}}}} \frac{\sigma}{\sqrt{p-1}} \\ s &= \sqrt{\Gamma G_N N_{\text{sol}}} \sqrt{p-1} t. \end{aligned}$$

Such a scaling reproduces the scaling behavior that we found numerically: The coupling strength  $K$  and the Lyapunov exponent (which scales inversely with time) scale with  $\sqrt{p-1}$ . The LK equations, Eqs. (1), can then be rewritten as

$$\begin{aligned} \frac{dE}{ds} &= \frac{1+i\alpha}{2} N E + K e^{i\theta} E (s - \sqrt{p-1} \tau) \\ \frac{dN}{ds} &= \frac{\gamma}{\Gamma} \left[ 1 - \frac{N}{c\sqrt{p-1}} - (c\sqrt{p-1} N + 1) |E|^2 \right] \end{aligned} \quad (18)$$

with  $c = \sqrt{G_N N_{\text{sol}}/\Gamma}$ . We assume small coupling strength  $K \ll 1$ , small carrier densities  $N = \mathcal{O}(K)$ , and a reasonably high pump current  $c\sqrt{p-1} = \mathcal{O}(1)$ . The ratio of photon and carrier life times,  $\gamma/\Gamma$ , is a small parameter as well. In leading order we obtain the following equations:

$$\begin{aligned} \frac{dE}{ds} &= \frac{1+i\alpha}{2} N E + K e^{i\theta} E (s - c\sqrt{p-1} \tau) \\ \frac{dN}{ds} &= \frac{\gamma}{\Gamma} (1 - |E|^2). \end{aligned} \quad (19)$$

These equations only depend on the pump current in the value of the time delay. Since the exact value of the time delay does not influence the sub-LE, we recover the scaling behavior found numerically. For increasing coupling strength  $K$  the mapping becomes less exact as can be seen in Fig. 6(c). This results from the fact that the rescaled model Eq. (19) is a weak coupling approximation.

### C. Auto-correlations and space-time patterns for strong and weak chaos

In this section we discuss the question whether the difference between strong and weak chaos can be identified

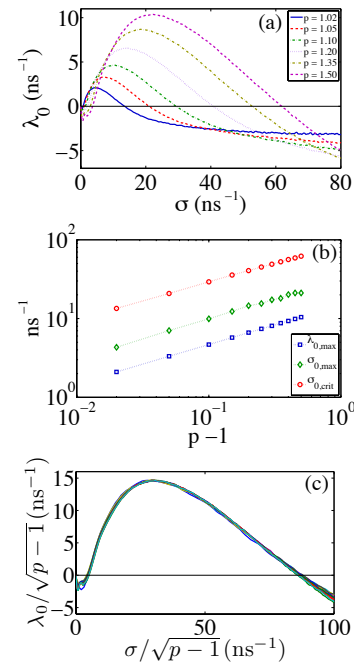


Figure 6. (Color online) (a) Sub-LE  $\lambda_0$  of a single laser with self-feedback for a delay time  $\tau = 10$  ns and several different pump currents  $p$  vs coupling strength  $\sigma$ . (b) Maxima  $\lambda_{0,\max}$  of the sub-LEs  $\lambda_0$ , coupling strengths  $\sigma_{0,\max}$  of these maxima, and critical coupling strengths  $\sigma_{\text{crit}}$  where  $\lambda_0 = 0$  for several different pump currents  $p$  vs effective pump current  $p - 1$  in double-logarithmic scale. (c) Data collapse of rescaled sub-LEs  $\lambda_0/\sqrt{p-1}$  vs rescaled coupling strengths  $\sigma/\sqrt{p-1}$  for eleven different pump currents  $p$  ranging from  $p = 1.02$  to  $p = 1.50$ .

from the laser time series itself. Fig. 7 shows two example trajectories (intensity traces) of a single laser with self-feedback for the regimes of weak and strong chaos. For both strong and weak chaos, there is a characteristic structure of high peaks which is significantly higher for weak chaos than for strong chaos. This may be caused by the larger coupling strength.

Fig. 8 shows the laser trajectories for weak and strong chaos in space-time diagrams where the vertical axis denotes the number of the current delay window of length  $\tau$  and the horizontal axis denotes the time offset  $t$  in this delay window. In such a representation, chaos evolves horizontally in space direction for strong chaos. This is due to the divergence between two nearby trajectories on the internal time scale of the laser which is much shorter than the delay time  $\tau$ . In contrast, weak chaos evolves vertically in the (discrete) time direction since the divergence between two nearby trajectories happens on the long time scale of the delay. Accordingly, the islands of high intensity (red) extend vertically farther in time direction for weak chaos than they do for strong chaos. In both kinds of visualization (intensity trace and space-time diagram), however, one cannot strictly distinguish between strong and weak chaos in a nonambiguous qual-

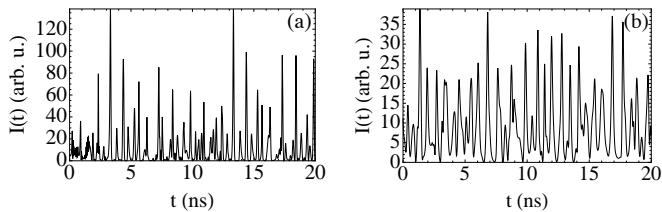


Figure 7. Example trajectories (intensity traces) of a single laser with a self-feedback of  $\tau = 10 \text{ ns}$  for (a) weak chaos ( $\sigma = 21 \text{ ns}^{-1}$ ) and (b) strong chaos ( $\sigma = 6 \text{ ns}^{-1}$ ) vs time  $t$ .

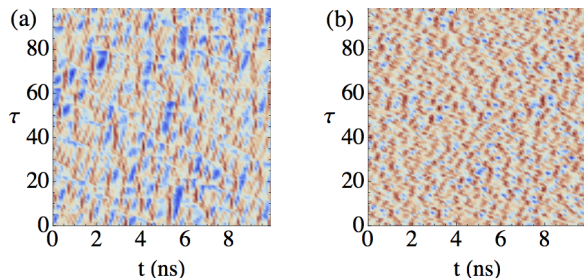


Figure 8. (Color online) Space-time diagram of a laser trajectory (reddish: high intensity, blueish: low intensity) for a single laser with a self-feedback of  $\tau = 10 \text{ ns}$  for (a) weak chaos ( $\sigma = 21 \text{ ns}^{-1}$ ) and (b) strong chaos ( $\sigma = 6 \text{ ns}^{-1}$ ) vs the number of the current delay window of length  $\tau$  (vertical axis) and the time offset  $t$  in this window (horizontal axis).

itative way.

Fig. 9 depicts the time-shifted auto-correlations  $C_{\text{auto}}$  of a single laser with self-feedback for the regimes of weak and strong chaos. For weak chaos, one clearly sees the high auto-correlation peaks at multiples of the delay time  $\tau$ . Although for strong chaos the chaotic behavior evolves predominantly on the internal time scale of the laser, whereas for weak chaos it evolves on the time scale of the delay, there are non-negligible auto-correlations after multiples of the delay time  $\tau$  even for strong chaos. However, they are significantly smaller than for weak chaos and decay faster with increasing time shift  $\Delta$ .

Considering the auto-correlations  $C_{\text{auto}, \Delta=\tau}$  after one delay time  $\tau$  in Fig. 10(a), we observe that they do not decay for large delay times with increasing  $\tau$  but remain constant. Surprisingly, this is not only the case

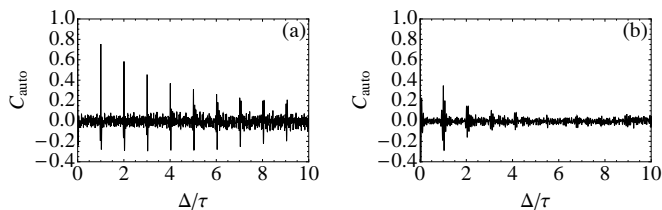


Figure 9. Time-shifted auto-correlations  $C_{\text{auto}}$  of a single laser with a self-feedback of  $\tau = 10 \text{ ns}$  for (a) weak chaos ( $\sigma = 21 \text{ ns}^{-1}$ ) and (b) strong chaos ( $\sigma = 6 \text{ ns}^{-1}$ ) vs time shift  $\Delta$  in units of the delay time  $\tau$ .

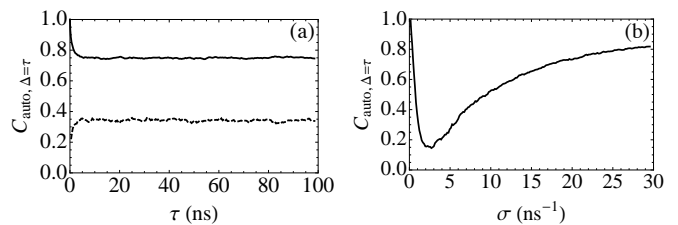


Figure 10. (a) Auto-correlations  $C_{\text{auto}}$  with a time shift of  $\Delta = \tau$  for a single laser with self-feedback for weak chaos ( $\sigma = 21 \text{ ns}^{-1}$ , solid line) and strong chaos ( $\sigma = 6 \text{ ns}^{-1}$ , dashed line) vs delay time  $\tau$ . (b) Auto-correlations  $C_{\text{auto}}$  with a time shift of  $\Delta = \tau$  for a single laser with a self-feedback of  $\tau = 10 \text{ ns}$  vs coupling strength  $\sigma$ .

for weak chaos but also for strong chaos. In Fig. 10(b) we depict the auto-correlations  $C_{\text{auto}, \Delta=\tau}$  with a time shift of one delay time  $\tau$  in dependence on the coupling strength  $\sigma$ . We find no sharp transition at the critical coupling strengths where the transitions between strong and weak chaos appears. For weak chaos, however, the auto-correlations  $C_{\text{auto}, \Delta=\tau}$  are significantly higher than for strong chaos.

We conclude that a linear measure like the auto-correlation function cannot clearly uncover the difference between strong and weak chaos. Instead, we propose the usage of nonlinear measures in order to detect a more significant difference in the relationship between  $\mathbf{x}(t)$  and  $\mathbf{x}(t - \tau)$ . The idea is motivated by the fact, that in weak chaos for sufficiently large delay times, the system can be considered to be in a state of generalized synchronization with its own time-delayed feedback, whereas in strong chaos the state of the system is formally independent of its input. Note that this independence does not imply the total absence of linear correlations, as we have demonstrated. The nature of the nonlinear functional dependence  $\mathbf{x}[\mathbf{x}_\tau]$  in weak chaos is exploited in the corresponding Abarbanel test as described in Sec. III A. Hence, the detection of strong and weak chaos from time series can be reduced to the problem of detecting generalized synchronization [21, 22]. We refer to the relevant methods used in this context, like the evaluation of nearest neighbors [23], mutual information or transfer entropy [24]. However, we assume severe computational difficulties regarding memory usage and runtime connected with the necessary delay embedding. Additionally, it might even be impossible to detect generalized synchronization from a finite time series.

#### D. External cavity modes for strong and weak chaos

We can relate the strongly or weakly chaotic behavior of a laser subjected to delayed feedback to the properties of the external cavity modes (ECMs) of the laser. These ECMs are rotating wave solutions of the LK equations of the form  $E(t) = E_0 e^{i\omega t}$  and  $n(t) = n$  with constant

amplitude  $E_0$ , frequency  $\omega$  and carrier density  $n$  of the laser. The spectrum of ECMs is often represented in the  $(\omega, n)$ -plane. In this plane the ECMs lie on an ellipse. ECMs located on the lower half are focus solutions called modes. The solutions located on the upper half of the ellipse are saddle points also referred to as antimodes.

Depending on the laser parameters, the ECMs have different stability properties. In the chaotic regime the ECMs can be seen as the skeleton of the chaotic attractor [25, 26]. In the low frequency fluctuations regime, which occurs for low pump currents and moderate to strong coupling strengths, the intensity slowly increases, followed by a sudden power dropout. During the buildup process, the trajectory travels along the modes in the direction of the maximal gain mode, until the trajectory is expelled along the unstable manifold of an antimode. This causes the power dropout. In the coherence collapse regime, the dynamics can be described as a chaotic itinerancy between modes and antimodes.

The stability can be calculated by inserting the ECM solution into Eq. (2). In the long delay limit, the characteristic equation of a steady state, such as the ECM solutions, has two types of solutions, which show a different scaling behavior with the delay time [27]. The strongly unstable spectrum consists of isolated points, which are approximated by the unstable eigenvalues of the Jacobian of the LK equations without delayed terms. These eigenvalues do not scale with the delay. Beside this strongly unstable spectrum, the characteristic equation has an infinite number of solutions, forming the pseudocontinuous spectrum. The real part of these solutions scales inversely with the delay.

One can thus distinguish between strongly and weakly unstable ECMs in an analogous way as we distinguish between strong and weak chaos. The local eigenvalues of the Jacobian without delay terms play a similar role as the sub-LE  $\lambda_0$ : Strongly unstable ECMs have unstable local eigenvalues, and thus a strongly unstable spectrum. The maximal eigenvalue is approximated by these local eigenvalues and does not change with the delay. The weakly unstable (and the stable) ECMs have stable local eigenvalues. The strongly unstable spectrum does not exist in this case, these ECMs only have a pseudocontinuous spectrum. Hence, the real part of the maximal eigenvalue scales inversely with the delay, just like the maximal LE  $\lambda_m$  for weak chaos [28].

In Fig. 11 we show the projection of the laser dynamics onto the external cavity modes. In the strongly chaotic regime, all the modes involved in the dynamics are strongly unstable, as illustrated in Fig. 11(a). Around the transition point between strong and weak chaos, a few (two or three) weakly unstable modes are involved in the dynamics, as shown in Fig. 11(b), while most of the modes involved in the dynamics are weakly unstable in the weakly chaotic regime, as shown in Fig. 11(c). These features are independent of the pump current. The antimodes are always strongly unstable, both in the weakly and strongly chaotic regime.

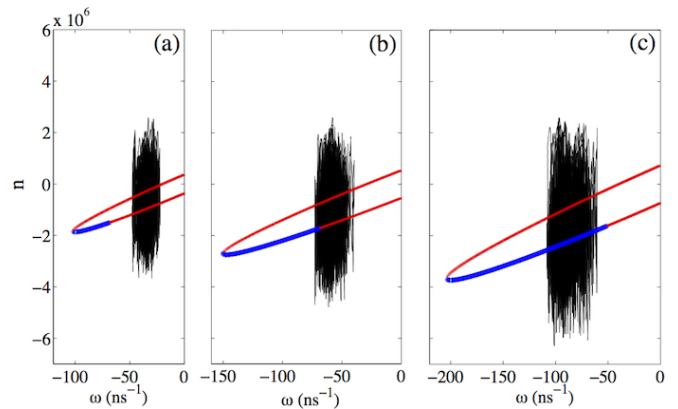


Figure 11. (Color online) Projection of the laser dynamics onto the  $(\omega, n)$ -plane for a delay time  $\tau = 10$  ns and a pump current  $p = 1.10$ . Thick blue dots denote weakly unstable or stable ECMs, thick red dots represent strongly unstable ECMs. Panel (a) shows a strongly chaotic trajectory for  $\sigma = 20$  ns $^{-1}$ . The modes and antimodes involved in the dynamics are strongly unstable. In panel (b) the dynamics around the transition point between strong and weak chaos is shown for  $\sigma = 29.28$  ns $^{-1}$ . The trajectory approximates the transition point between weakly and strongly unstable modes on the ellipse. Panel (c) shows weakly chaotic laser dynamics for  $\sigma = 40$  ns $^{-1}$ . All the modes involved in the dynamics are weakly unstable.

### E. Sub-Lyapunov exponents for two self-feedbacks with time-scale separated delays

Until now we have only considered a single laser with self-feedback and have discussed the sub-LE in this context. Now we generalize our investigation by introducing a second self-feedback which has a delay time that is much smaller than the first one. The linearized equation describing the maximal LE is

$$\delta \dot{\mathbf{x}} = DF(\mathbf{x}) \delta \mathbf{x} + \sigma_s DH(\mathbf{x}_{\tau_s}) \delta \mathbf{x}_{\tau_s} + \sigma_l DH(\mathbf{x}_{\tau_l}) \delta \mathbf{x}_{\tau_l} \quad (20)$$

where  $\tau_s$  is the delay time of the shorter self-feedback in comparison with the longer self-feedback with delay time  $\tau_l$ . Additionally to the sub-LE  $\lambda_0$  defined from Eq. (7) we introduce another sub-LE  $\lambda_{0,s}$  defined from

$$\delta \dot{\mathbf{x}}_{0,s} = DF(\mathbf{x}) \delta \mathbf{x}_{0,s} + \sigma_s DH(\mathbf{x}_{\tau_s}) \delta \mathbf{x}_{0,s,\tau_s}. \quad (21)$$

Thus, for  $\lambda_{0,s}$  we consider a subsystem which includes the shorter self-feedback but omits the longer one in the linearized equation. As before, the inserted dynamics  $\mathbf{x}(t)$  is the trajectory of the full system which includes both the long and the short self-feedbacks.

Fig. 12(a) shows the sub-LEs  $\lambda_0$  and  $\lambda_{0,s}$  together with the maximal LE  $\lambda_m$  for the case when  $\tau_l$  is much larger than  $\tau_s$  such that we have a time scale separation between the two delays. We observe that  $\lambda_{0,s} < \lambda_0$  holds for strong chaos and  $\lambda_{0,s} > \lambda_0$  for weak chaos. Furthermore,  $\sigma_{\text{crit},0} \approx \sigma_{\text{crit},0,s}$  holds for the right transition at large  $\sigma$ , i. e. both sub-LEs change their signs at approximately the same coupling strength and can hence both

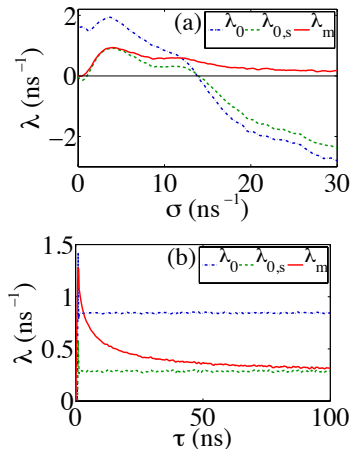


Figure 12. (Color online) Maximal LE  $\lambda_m$  (solid line) and sub-LEs  $\lambda_{0,s}$  and  $\lambda_0$  (dashed and dotted lines) for a single laser with two self-feedbacks  $\tau_1$  and  $\tau_s$  for (a)  $\tau_1 = 10$  ns,  $\tau_s = 0.1$  ns and  $\sigma_s = 5$  ns $^{-1}$  vs coupling strength  $\sigma := \sigma_1$  and (b)  $\tau_s = 0.1$  ns,  $\sigma_s = 5$  ns $^{-1}$  and  $\sigma_1 = 10$  ns $^{-1}$  (strong chaos) vs delay time  $\tau := \tau_1$ .

be used as an indicator for strong or weak chaos there. For small  $\sigma$ , however, only  $\lambda_{0,s}$  changes its sign indicating the transitions between weak and strong chaos there. Thus,  $\lambda_{0,s}$  is the new relevant sub-LE which determines the occurrence of strong or weak chaos in a system with two time-scale separated delays. This is confirmed by Fig. 12(b) which shows that in the regime of strong chaos,  $\lambda_m \rightarrow \lambda_{0,s}$  holds for increasing  $\tau_1$ , while for weak chaos,  $\lambda_m \sim 1/\tau_1$ .

## V. NETWORKS OF LASERS WITH TIME-DELAYED COUPLINGS

### A. The master stability formalism

We investigate complete chaotic synchronization of  $N$  identical coupled laser elements. The state of each element is described by  $\mathbf{x}^i$  with  $i = 1 \dots N$ . We start from the physically motivated ansatz

$$\dot{\mathbf{x}}^i = \mathbf{F}(\mathbf{x}^i) + \sigma \sum_{j=1}^N G^{ij} \mathbf{H}(\mathbf{x}_\tau^j). \quad (22)$$

The matrix  $G \in \mathbb{R}^{N \times N}$  contains the network topology.  $G^{ij}$  is the normalized coupling strength with which the laser  $i$  receives input from laser  $j$ . In order to guarantee the existence of the completely synchronized state  $\mathbf{x}^1(t) = \mathbf{x}^2(t) = \dots = \mathbf{x}^N(t) := \mathbf{s}(t)$ , the row sum of  $G$  has to be constant for all rows, and we choose  $\sum_j G^{ij} = 1$ . Then the synchronized state  $\mathbf{s}(t)$  reduces Eq. (22) to

$$\dot{\mathbf{s}} = \mathbf{F}(\mathbf{s}) + \sigma \mathbf{H}(\mathbf{s}_\tau). \quad (23)$$

The stability properties of the synchronized state  $\mathbf{s}(t)$  are well-described by the master stability formalism from Pecora and Carroll [29]. For completeness, we summarize the main ideas introduced in their work. A small perturbation is applied to the synchronized state, such that  $\mathbf{x}^i(t) = \mathbf{s}(t) + \delta \mathbf{x}^i(t)$ . The equations of motion are then linearized around  $\mathbf{s}(t)$  and the perturbations obey the equations of motion

$$\dot{\delta \mathbf{x}}^i = DF(\mathbf{s}) \delta \mathbf{x}^i + \sigma \sum_{j=1}^N G^{ij} DH(\mathbf{s}_\tau) \delta \mathbf{x}_\tau^j. \quad (24)$$

This set of equations can be decoupled into the amplitudes  $\xi^k(t)$  of the network eigenmodes  $\mathbf{g}^k \in \mathbb{R}^N$ , for which  $G \cdot \mathbf{g}^k = \gamma_k \mathbf{g}^k$  and  $k = 1 \dots N$ . With  $\delta \mathbf{x}^i = \sum_k g^{k,i} \xi^k$  we obtain  $N$  decoupled equations

$$\dot{\xi}^k = DF(\mathbf{s}) \xi^k + \sigma \gamma_k DH(\mathbf{s}_\tau) \xi_\tau^k. \quad (25)$$

Integration of this equation for the  $k$ -th perturbation mode  $\mathbf{g}^k$  yields the maximal LE  $\lambda_k$ , which tells us about the stability of the mode, meaning that a perturbation  $\delta \mathbf{x}(t) = (\delta \mathbf{x}^1(t), \delta \mathbf{x}^2(t), \dots, \delta \mathbf{x}^N(t))$  in direction of  $\mathbf{g}^k$  grows or decays exponentially. By construction, there exists at least  $\gamma_1 = 1$  with the eigenvector  $\mathbf{g}^1 = (1, 1, \dots, 1)^\top$ , which corresponds to a perturbation  $\delta \mathbf{x}(t) = \delta \mathbf{s}(t)$  within the SM. It determines, whether the synchronous dynamics is chaotic ( $\lambda_1 > 0$ ) or not. The other modes correspond to linear combinations of differences between the laser elements and therefore the necessary condition to find stable complete synchronization is  $\lambda_k < 0$  for  $k = 2 \dots N$ . Since all  $|\gamma_k| \leq 1$ , the knowledge of the master stability function  $\lambda(\gamma)$  is sufficient to predict, whether a network of coupled lasers described by the coupling matrix  $G$  is able to display complete synchronization or not.

### B. Master stability function for weak chaos

Here we show the general master stability function for the limit of large delays in weak chaos. To this end, we make use the scaling behavior  $\lambda_m = \mathcal{O}(\tau^{-1})$ . The initial point of our considerations is a generalization of Eq. (25), which reads

$$\dot{\mathbf{y}} = A(t) \mathbf{y} + \kappa B(t) \mathbf{y}_\tau, \quad (26)$$

where  $A(t) := DF[\mathbf{s}(t)]$  and  $B(t) := DH[\mathbf{s}(t - \tau)]$ . The exponent  $\lambda_{\mathbf{y}}(\kappa)$  provides the master stability function. Transformation with  $\mathbf{z} = \exp(-\lambda_{\mathbf{y}} t) \mathbf{y}$  yields a system with exponent  $\lambda_{\mathbf{z}} = 0$

$$\dot{\mathbf{z}} = (A(t) - \lambda_{\mathbf{y}} \cdot \mathbb{1}) \mathbf{z} + \kappa e^{-\lambda_{\mathbf{y}} \tau} B(t) \mathbf{z}_\tau. \quad (27)$$

Weak chaos has the important property, that by changing  $A(t) \rightarrow A'(t) = \mathbf{A}(t) + \varepsilon \cdot \mathbb{1}$  with  $\varepsilon \in \mathbb{R}$  and  $|\varepsilon| < \lambda_0$ , we affect the LE only in the order of  $\tau^{-1}$ . Therefore, if  $\varepsilon$  itself is decreasing with  $\tau$ , the effect on the exponent is

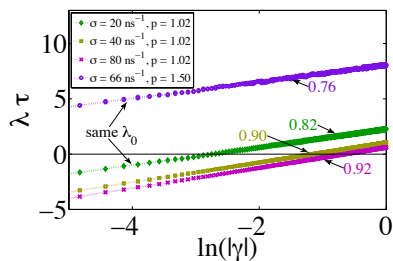


Figure 13. (Color online) Product  $\lambda \cdot \tau$  of the master stability function  $\lambda(\gamma)$  and the delay time  $\tau = 10$  ns for the SM and several different coupling strengths  $\sigma$  and pump currents  $p$  in weak chaos regime vs  $\ln(|\gamma|)$ .

of a smaller order in  $\tau$ , i.e.  $\mathcal{O}(\tau^p)$  with  $p < -1$ . Then for sufficiently large  $\tau$ , removing  $\lambda_{\mathbf{y}}$  from the first term on the RHS of Eq. (27) leads to

$$\dot{\mathbf{y}}' = A(t) \mathbf{y}' + \kappa e^{-\lambda_{\mathbf{y}} \tau} B(t) \mathbf{y}'_{\tau}, \quad (28)$$

with the exponent  $\lambda'_{\mathbf{y}} = \mathcal{O}(\tau^p)$ . Comparison of the equivalent Eqs. (26) and (28) shows, that in the *leading* order of  $\tau^{-1}$ , rescaling of the coupling strength  $\kappa \rightarrow \kappa' = \kappa \exp(-\lambda_{\mathbf{y}} \tau)$  led to an exponent  $\lambda'_{\mathbf{y}} \approx 0$ . From the knowledge of the zero-crossing at  $\kappa'$ , we directly obtain the scaling law

$$\lambda_{\mathbf{y}}(\kappa) = \frac{1}{\tau} \ln \frac{\kappa}{\kappa'}. \quad (29)$$

Although in general the value of  $\kappa'$  is unknown, this logarithmic law allows us to connect the maximal LE of the SM with the stability of all transversal modes of a network. We refer to Eq. (25), in which  $\kappa = \sigma \gamma_k$ . Assume the maximal LE  $\lambda_m = \lambda_1$  of the SM is known. It corresponds to  $\gamma_1 = 1$ , so  $\lambda_m = \lambda_1 = \lambda(\sigma \cdot 1)$  is the point at which we can fix the master stability function. Then for an arbitrary  $\gamma_k$  we obtain from Eq. (29) the exponent

$$\lambda(\sigma \gamma_k) = \lambda_m + \ln |\gamma_k|. \quad (30)$$

Here we have made use of the fact, that the exponent depends only on the absolute value  $|\kappa|$  for large delays. This scaling relation also holds for steady states [14]. Transversal stability of the  $k$ -th mode is given if  $\lambda(\sigma \gamma_k) < 0$ . This leads to the synchronization criterion

$$|\gamma_k| < e^{-\lambda_m \tau}, \quad (31)$$

which connects transversal and longitudinal stability in a network exhibiting weak chaos.

### C. Master stability function for the Lang-Kobayashi dynamics

We now investigate the master stability function  $\lambda(\gamma)$  for the LK equations dynamics. For strong chaos,  $\lambda(\gamma)$  is constant since the delay term becomes exponentially

small in the master stability equation (25) for  $\tau \rightarrow \infty$ . Hence, any perturbation mode with eigenvalue  $\gamma$  in a network, or the mode for complete synchronization in any arbitrary network, respectively, is unstable for strong chaos if the delay time is large. Consequently, complete synchronization of networks with identical, strongly chaotic units is excluded on principle for  $\tau \rightarrow \infty$ .

For weak chaos,  $\lambda(\gamma)$  basically exhibits a logarithmic dependence on  $\gamma$ . However, we observe two deviations that can be considered as effects of the finiteness of the delay time  $\tau$  which is present in every experiment or simulation. As a first deviation,  $\lambda(\gamma)$  does not diverge to  $-\infty$  for  $\gamma \rightarrow 0$  but has a finite value  $\lambda(0)$ : the sub-LE  $\lambda_0$ . It is important to note here that the sub-LE  $\lambda_0$  is equal to the LE of any perturbation mode with  $\gamma = 0$  of a network (e.g. the mode of complete synchronization of the two outer lasers in a bidirectionally coupled chain of three lasers) since then the delay term drops out in the master stability equation (25), too. This is also the case in the experimental setup for the measurement of the sub-LE presented in Fig. 1(a). There, the mode of complete synchronization has  $\gamma = 0$ , and hence synchronization between the two laser happens if and only if they show weakly chaotic behavior.

As a second deviation for weak chaos, Fig. 13 shows for several different coupling strengths and pump currents that the exponent  $\nu$  in  $\lambda \sim \ln(|\gamma|^\nu) = \nu \cdot \ln(|\gamma|)$  is not exactly One as for simple analytic models with constant coefficients, but rather shows some deviation to exponents smaller than One. We were able to find this deviation also for the Lorenz dynamics. For constant delay time  $\tau$  and constant laser pump current  $p$ , the exponent gets closer to One the larger  $\sigma$  is, i.e. the weaker the chaos becomes. Additionally, if the coupling strength  $\sigma$  is adjusted such that the sub-LE  $\lambda_0$  is the same for two different pump currents, then the slope is closer to One for a small pump current than for a higher pump current. As presented in the previous section, a condition for the prediction of synchronization in a network, Eq. (31), can be derived from the behavior of  $\lambda(\gamma)$ . Due to the empirically observed slope smaller than One, this condition should be refined to

$$|\gamma_2| < e^{-\lambda_m \tau / \nu} \quad (32)$$

where  $\gamma_2$  is the eigenvalue of the coupling matrix  $G$  with the second largest modulus. This equation allows for a more precise practical prediction of synchronization in networks of semiconductor lasers, derived from LK equation modeling.

### D. Experimental evidence of strong and weak chaos in bidirectionally delay-coupled lasers

In a system with two bidirectionally delay-coupled lasers without self-feedback or multiple delays, identical chaos synchronization is not stable due to symmetry

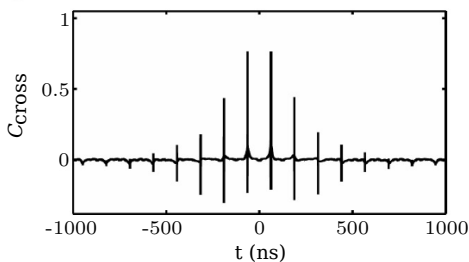


Figure 14. Cross-correlation function of two bidirectionally delay-coupled lasers in the chaotic regime ( $\tau = 63$  ns).

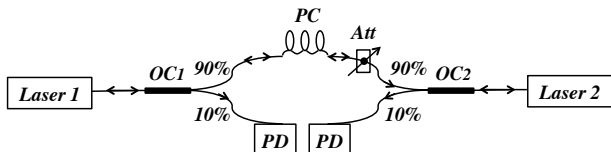


Figure 15. Fiber-based experimental setup of two mutually delay-coupled semiconductor lasers.  $OC_{1,2}$  stand for the optical couplers,  $PC$  is the polarization controller,  $Att$  is the variable attenuator, and  $PD$  denotes the photodetectors.

breaking [30]. However, chaos synchronization can still exist in the generalized sense [19]. Here, we give experimental and numerical evidence that the implications of strong and weak chaos regimes also apply to the case of generalized chaos synchronization.

In the context of delay-coupled elements, correlation measures can fail to detect synchronization if the number of coupled elements is large [22]. However, the cross-correlation function is still a good indicator to identify generalized synchronization between two delay-coupled lasers. We present an example of such a cross-correlation function in Fig. 14, which shows distinct peaks at the delay time  $\tau$  and its odd multiples. In this figure, the large correlation peak at the delay time indicates that the lasers are generally synchronized. We argue that generalized chaos synchronization is only possible, if the lasers are operating in the weak chaos regime. In contrast, a low correlation peak at a time-lag  $\tau$  is to be expected, if the lasers are operating in the strong chaos regime.

Our fiber-optics-based experimental arrangement is schematically shown in Fig. 15. We use two single-mode, fiber-pigtailed, discrete-mode semiconductor lasers, emitting at 1542 nm. The lasers have been hand-selected in order to achieve well-matched parameters. The laser temperatures and currents are stabilized to an accuracy of 0.01 K and 0.01 mA, respectively. The lasers are biased at a current of  $1.25 I_{th}$ , with  $I_{th} = 11.7$  mA being the solitary laser threshold current. As shown in Fig. 15, the coupling path includes two 90/10 optical couplers  $OC_{1,2}$ , a polarization controller  $PC$ , and an optical attenuator  $Att$ . The maximum mutual coupling obtained in this experimental arrangement can be estimated to be  $\sim 40\%$  of the emitted light. The 10% outputs of  $OC_{1,2}$  are used for detection.

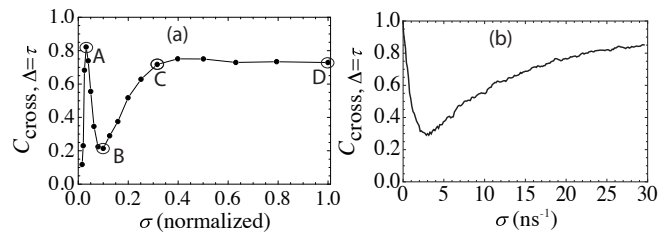


Figure 16. (a) Experimentally measured and (b) numerically calculated cross-correlations  $C_{cross}$  with a time shift of  $\Delta = \tau$  for a bidirectionally coupled pair of lasers as a function of the coupling strength  $\sigma$ . The delay time is  $\tau = 10$  ns in the numerics and  $\tau = 63$  ns in the experiments, corresponding to the long delay limit. The experimental coupling strength is normalized to the maximum coupling obtained in the setup, which is about 40% of the emitted light.

The values of the cross-correlation between the intensities emitted by Lasers 1 and 2 for a time shift of  $\tau$  are shown in Fig. 16(a) as a function of the coupling strength  $\sigma$ . For strong couplings  $\sigma > 0.3$ , a region of large correlation is found. Decreasing the coupling strength to  $0.1 < \sigma < 0.3$  results in a sudden decrease of the correlation. A second region of large correlation can be identified for weak couplings  $\sigma \sim 0.05$ . The correlation decreases again for the weakest couplings  $\sigma < 0.05$ . The numerical results, shown in Fig. 16(b), agree with the experimental results. For large couplings, the two coupled lasers are highly correlated. A distinct region of low correlation can be seen for intermediate couplings, while the correlation increases again for the weakest coupling strengths. The numerical simulations do not reproduce the correlation decrease towards zero coupling since spontaneous emission noise sources are not considered. The numerical results of the time-shifted cross-correlations for the two bidirectionally coupled lasers shown in Fig. 16(b) are similar to the auto-correlations of a single laser with self-feedback shown in Fig. 10(b). The parameters used in the numerical simulations are listed in the appendix.

Several dynamical states are being observed for variation of the coupling along the correlation curve in Fig. 16(a). The lasers operate in continuous-wave with noisy fluctuations in the absence of coupling. For an increasing coupling strength, the lasers follow a quasi-periodic route via undamped relaxation oscillations reaching a chaotic state at point A. The delay-induced dynamics produces a dramatic increase in the laser optical linewidth, which increases from a few MHz to several GHz due to the coupling. We present in Fig. 17 the typical shape of the optical spectra of the chaotic laser for points denoted as B and C in Fig. 16(a). These two spectra are qualitatively similar apart from their different width, but correspond to significantly different correlation and synchronization properties. In order to characterize the optical spectra, we have measured their width, defined as the  $-20$  dB frequency width. The  $-20$  dB width of the optical spectrum is 9 GHz, 20 GHz, 26 GHz,

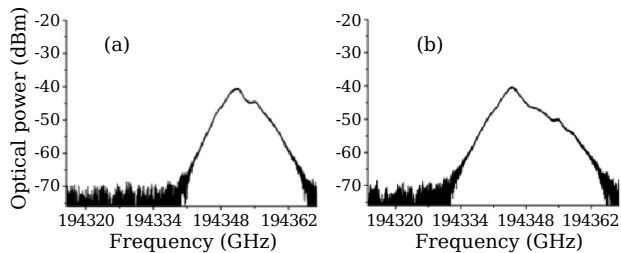


Figure 17. Optical spectra for points denoted as (a)  $B$  and (b)  $C$  in Fig. 16(a).

and 35 GHz, for points  $A$ ,  $B$ ,  $C$ , and  $D$ , respectively.

We observe irregular (chaotic) dynamics in the whole range from  $A$  to  $D$ . However, the correlation plot indicates qualitative transitions of the synchronization behavior between  $A$  and  $B$ , and  $B$  and  $C$ , respectively. More precisely, the experimental correlation plot shows a large correlation around  $A$ , and from  $C$  to  $D$ , indicating that the lasers are generally synchronized in these regions. The degree of synchronizability stems from the dynamical regime the lasers are operating in. Therefore, we can infer that the lasers operate in a weak chaos regime in the two high correlation (synchronization) regions, i. e. for  $\sigma > 0.3$  and  $\sigma \sim 0.05$ . In contrast, a region of low correlation measure can be seen for intermediate couplings  $\sigma \sim 0.1$ . This can be associated with a strong chaos dynamical regime. The numerical correlation plot shows a similar clear distinction between different correlation regions, with a window of low correlation around  $\sigma \sim 2.5 \text{ ns}^{-1}$ . This low correlation can be linked to a strong chaos dynamical regime.

Our experimental results on two delay-coupled semiconductor lasers presented here support the sequence ‘weak to strong to weak chaos’ with an increasing coupling strength. Even though the master stability function cannot be directly applied to the generally synchronized solution, the influence of the dynamical regime on the synchronization is clearly substantiated by our experimental and numerical results.

### E. Networks with several distinct sub-Lyapunov exponents

In a network we can define a sub-LE for each individual unit. If the network is not completely symmetric then these sub-LEs may differ from each other, even if the units by themselves are identical. For example, in a chain of three bidirectionally coupled lasers, the middle laser is in a different coupling situation than the outer lasers. It receives input from two lasers while the outer ones receive input only from one laser. It is important to note here that the accumulated coupling strength of the inputs, however, is constant for each laser of the chain. The occurrence of strong or weak chaos now depends on both sub-LEs present in the network. Fig. 18(a) shows that this dependence is simple: The maximal sub-LE of the

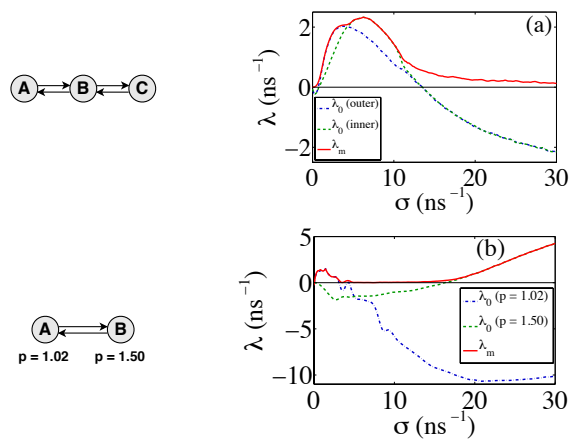


Figure 18. (Color online) (a) Maximal LE  $\lambda_m$  (solid line) and sub-LEs  $\lambda_0$  of the inner laser (dashed line) and the outer lasers (dot-dashed line) of a chain of three lasers (see left) for a coupling delay time of  $\tau = 10 \text{ ns}$  vs coupling strength  $\sigma$ . (b) Maximal LE  $\lambda_m$  (solid line) and sub-LEs  $\lambda_0$  (dashed and dot-dashed lines) of pair of two lasers with distinct pump currents (see left) for a coupling delay time of  $\tau = 10 \text{ ns}$  vs coupling strength  $\sigma$ .

network determines whether there is strongly or weakly chaotic behavior of the complete network’s maximal LE. If the largest  $\lambda_0$  in the network is negative then there is weak chaos, if the largest  $\lambda_0$  in the network is positive, then the maximal LE  $\lambda_m$  of the network converges to the maximal sub-LE of the network. This means that potentially additionally present strongly chaotic units do not further increase the value to which the complete network’s maximal LE converges for strong chaos.

Additionally to the case when the network is not completely symmetric, also the individual units in the network may be nonidentical, e. g. in a pair of two bidirectionally coupled lasers with different pump currents, Fig. 18(b). One laser has a pump current  $p = 1.02$  and the other has  $p = 1.50$ . It is confirmed that even for this case, the largest sub-LE of the network determines the maximal LE of the network and that for strong chaos the maximal LE of the network follows the largest sub-LE. We further observe that, by making the lasers in the network nonidentical, we can even induce more transitions between strong and weak chaos than the transition weak/strong/weak chaos for a single laser or a network of identical lasers as shown before. These additional transitions are interrupted by intervals of  $\sigma$  where the maximal LE  $\lambda_m$  decays to Zero, i. e. windows of periodic behavior can be found.

As a consequence, we conclude that complete synchronization is excluded on principle for arbitrary networks which contain at least one strongly chaotic unit if the delay time is very large. Cluster synchronization, however, is still possible. In this case, the weakly chaotic units of the network may form one or more clusters. These clusters are driven by the strongly chaotic units of the network.

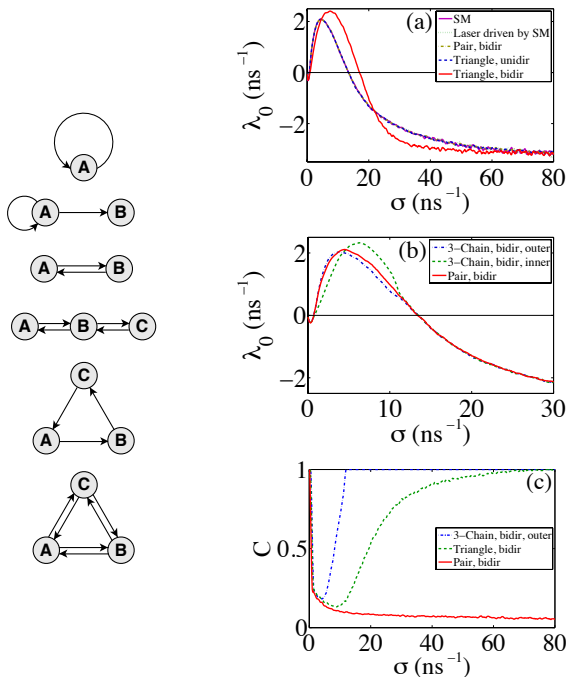


Figure 19. (Color online) (a) Sub-LEs  $\lambda_0$  for several network patterns where the lasers receive input from one laser (see left) in comparison with  $\lambda_0$  of a bidirectional triangle of lasers for a coupling delay time  $\tau = 10$  ns vs coupling strength  $\sigma$ . (b) Sub-LEs  $\lambda_0$  of the inner and outer lasers of a chain of three lasers in comparison with  $\lambda_0$  of a pair of lasers (see left) for a coupling delay time  $\tau = 10$  ns vs coupling strength  $\sigma$ . (c) Cross-correlation  $C$  between the lasers in several network patterns for a coupling delay time  $\tau = 10$  ns vs coupling strength  $\sigma$ .

### F. Sub-Lyapunov exponents for certain network patterns

In the previous section we have shown that different number of inputs from other lasers and their arrangement can have the effect of distinct sub-LEs. This is the case even if the lasers by themselves are identical. In this section we address the question if the number of inputs is the only criterion which determines the sub-LE for otherwise constant system parameters. We would like to emphasize once more that the accumulated coupling strength of the inputs is constant for all considered network patterns.

Fig. 19(a) shows a comparison of the sub-LEs of several networks where each laser receives input from exactly one laser. The SM, represented by a single laser with self-feedback, and the bidirectionally coupled pair, for which the experimental evidence of strong and weak chaos has been provided in Sec. V D, can be seen as limit cases of unidirectional rings containing one and two lasers. They are compared with a unidirectional triangle which is a unidirectional ring of three lasers. The bidirectional pair and the unidirectional triangle have in common that they do not have an eigenvalue gap. Hence, they cannot syn-

chronize isochronously for any coupling strength  $\sigma$  as shown in Fig. 19(c) for the example of the bidirectional pair. Nevertheless, their sub-LEs are exactly the same as the one of the SM represented by a single laser with self-feedback. Also the sub-LE of Laser  $B$  of the configuration presented in Fig. 1(a) is equal to the ones mentioned before even in the strong chaos regime where the Laser  $B$  is not synchronized with Laser  $A$ . The reason for this is that in all cases the lasers receive coherent input from a single source which exhibits the specific statistics of a laser trajectory. It does not matter if the statistics comes from a synchronized laser or an unsynchronized one, as long as it is typical for a single laser. This can also be nicely seen in Fig. 19(a) by the sub-LE of a bidirectionally coupled triangle. If the coupling strength  $\sigma$  is not large enough to induce synchronization of this triangle configuration, as seen in Fig. 19(c), then each laser receives incoherently superimposed input from two unsynchronized lasers. Hence, the sub-LE of the bidirectional triangle is then different from the sub-LEs of the networks with input from one laser. As soon as the bidirectional triangle synchronizes, however, its sub-LE becomes equal to the networks with input from one laser. The reason is that the signals from the two other laser are superimposed coherently and thus equal the signal from one laser.

Fig. 19(b) shows the two distinct sub-LEs of the inner and outer lasers of a chain of three bidirectionally coupled lasers in comparison with the sub-LE of the bidirectional pair. If the coupling strength  $\sigma$  is large enough for the outer lasers to synchronize, as seen in Fig. 19(c), then the inner laser receives the coherent superposition of the signals of the outer lasers. Thus, all three lasers in the chain effectively receive input from one unsynchronized laser. In consequence, the chain can be reduced to a bidirectional pair of unsynchronized lasers. Indeed, Fig. 19(b) confirms that the sub-LEs of the outer and inner lasers of the chain become identical and also equal to the sub-LE of the bidirectional pair in this regime.

Fig. 20(a) shows a comparison of the sub-LEs of several network configurations (depicted on the left side) in which the lasers receive input from two other lasers. Fig. 20(b) shows a comparison of the sub-LEs of several networks (depicted on the left side) where the lasers receive input from three other lasers. In both diagrams it turns out that for small coupling strengths in a partial range of the strong chaos regime, the sub-LE indeed only depends on the number of inputs and is equal for networks which have the same number of inputs. For larger coupling strengths, however, the sub-LEs differ from each other. The reason for this is that the two or three inputs correspond to an incoherent superposition of two or three laser signals. The level of coherence or incoherence depends on the topology of the subnetwork from which the signals originate. These different levels of incoherence play a larger role for the laser receiving the signals for increasing coupling strength.

Fig. 20(c) shows a comparison of the sub-LEs of a laser which receives unidirectional input from one, two or three mutually uncoupled lasers with self-feedback. The influ-

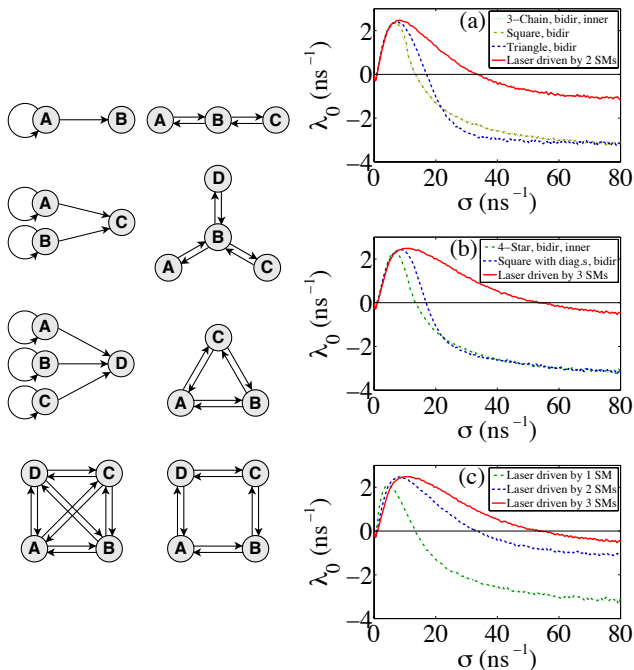


Figure 20. (Color online) (a) Sub-LEs  $\lambda_0$  for several network patterns where the lasers receive input from two lasers (see left) for a coupling delay time  $\tau = 10$  ns vs coupling strength  $\sigma$ . (b) Sub-LEs  $\lambda_0$  for several network patterns where the lasers receive input from three lasers (see left) for a coupling delay time  $\tau = 10$  ns vs coupling strength  $\sigma$ . (c) Sub-LEs  $\lambda_0$  of a laser driven by one, two or three independent laser with self-feedback for a coupling delay time  $\tau = 10$  ns vs coupling strength  $\sigma$ .

ence of the topology of the subnetwork from which the laser receives the two or three signals is eliminated by the fact that the two or three driving lasers are completely independent from each other. Also, the driven laser does not feed back any signal to the driving lasers. Hence, Fig. 20(c) shows the dependence of the sub-LE on the number of the completely incoherently superimposed inputs. For increasing number of inputs, the statistics of the received summed signal gets less similar to the one of a laser and increasingly similar to noise. We observe that with increasing number of inputs, the sub-LE gets larger for large coupling strengths  $\sigma$  and smaller for small  $\sigma$ .

## VI. SUMMARY

In this paper we have extended the investigations on strong and weak chaos of [17] by focusing on the dynamics of semiconductor lasers. After describing the LK equations and their linearization as a model for the numerical simulation of a semiconductor laser with time-delayed couplings, we have introduced the artificial sub-LE  $\lambda_0$  and have explained how to determine its sign by experiments.

Strong and weak chaos show different scaling proper-

ties of the maximal LE with the delay time. The sign of the sub-LE  $\lambda_0$  distinguishes between strong and weak chaos. The transition sequence ‘weak to strong chaos and back to weak chaos’ upon monotonically increasing the coupling strength  $\sigma$  of a single laser’s self-feedback has been shown for numerical calculations of the LK equations. At the transition between strong and weak chaos, the sub-LE vanishes,  $\lambda_0 = 0$ . At this transition we found  $\lambda_m \tau \sim \sqrt{\tau}$ . Transitions between strong and weak chaos by changing  $\sigma$  could also be found for the Rössler and Lorenz dynamics.

Counterintuitively, the difference between strong and weak chaos is not directly visible from the trajectory although the difference of the trajectories induces the transitions between the two types of chaos. In addition, a linear measure like the auto-correlation function cannot unambiguously reveal the difference between strong and weak chaos, either. Although the auto-correlations after one delay time are significantly higher for weak chaos than for strong chaos, it was not possible to detect a qualitative difference. But we could relate the trajectories of strong and weak chaos to the properties of the external cavity modes of the laser. If two time-scale separated self-feedbacks are present, the shorter feedback has to be taken into account for the definition of a new sub-LE  $\lambda_{0,s}$  which in this case determines the occurrence of strong or weak chaos. We have shown that the sub-LE scales with the square root of the effective pump current  $\sqrt{p-1}$ , as well in its magnitude as in the position of the critical coupling strengths.

For networks of delay-coupled lasers, we explained using the master stability formalism the condition  $|\gamma_k| < e^{-\lambda_m \tau}$  for stable chaos synchronization. Hence, synchronization of any network depends only on the properties of a single laser and the eigenvalue gap of the coupling matrix. We refined the master stability function for the LK dynamics to allow for precise practical prediction of synchronization. We provided the first experimental evidence of strong and weak chaos in bidirectionally delay-coupled lasers which supports the sequence ‘weak to strong to weak chaos’. For networks with several distinct sub-LEs it has been shown that the maximal sub-LE of the network determines whether the network’s maximal LE scales strongly or weakly with increasing delay time. As a consequence, complete synchronization of a network is excluded for arbitrary networks which contain at least one strongly chaotic laser. Finally, we showed that the sub-LE of a driven laser depends on the number of the incoherently superimposed inputs from desynchronized input lasers.

## ACKNOWLEDGMENTS

We thank the Deutsche Forschungsgemeinschaft and the Leibniz-Rechenzentrum in Garching, Germany, for their support of this work. M. C. S. and I. F. acknowledge the support by MICINN (Spain) under project DeCoDicA (TEC2009-14101).

### Appendix A: Parameters for the simulation of the Lang-Kobayashi equations

If not mentioned differently in the text, the constants listed in Tab. I were used in the simulation of the LK equations.

Table I. Used constants in the simulation of the LK equations. Values are taken from [31].

Parameter	Symbol	Value
Linewidth enhancement factor	$\alpha$	5
Differential optical gain	$G_N$	$2.142 \times 10^4 \text{ s}^{-1}$
Laser frequency	$\omega_0$	$2\pi c/(635 \text{ nm})$
Pump current relative to $J_{\text{th}}$	$p$	1.02
Threshold pump current of solitary laser	$J_{\text{th}}$	$\gamma N_{\text{sol}}$
Carrier decay rate	$\gamma$	$0.909 \times 10^9 \text{ s}^{-1}$
Carrier number of solitary laser	$N_{\text{sol}}$	$1.707 \times 10^8$
Cavity decay rate	$\Gamma$	$0.357 \times 10^{12} \text{ s}^{-1}$

### Appendix B: Critical coupling strengths in dependence on the pump current

Tab. II lists the critical coupling strengths for which  $\lambda_0 = 0$  and at which the transitions from weak to strong chaos and from strong to weak chaos appear, in dependence on the pump current  $p$ .

Table II. Critical coupling strengths where  $\lambda_0 = 0$  and at which the transitions from weak to strong chaos ( $\sigma_{\text{crit},1}$ ) and from strong to weak chaos ( $\sigma_{\text{crit},2}$ ) happen in dependence on the pump current  $p$ .

$p$	$\sigma_{\text{crit},1} \text{ (ns}^{-1}\text{)}$	$\sigma_{\text{crit},2} \text{ (ns}^{-1}\text{)}$
1.02	0.80	13.44
1.05	0.96	20.80
1.10	1.44	29.28
1.15	1.76	35.68
1.20	2.08	40.64
1.25	2.40	45.12
1.30	2.72	48.96
1.35	2.88	52.64
1.40	3.20	56.16
1.45	3.36	58.88
1.50	3.68	61.92

- [1] R. Albert and A.-L. Barabási, *Rev. Mod. Phys.* **74**, 47 (2002).
- [2] S. Boccaletti *et al.*, *Phys. Rep.* **424**, 175 (2006).
- [3] A. Arenas *et al.*, *Phys. Rep.* **469**, 93 (2008).
- [4] C. Song *et al.*, *Science* **327**, 1018 (2010).
- [5] R. Vardi *et al.*, *EPL (Europhysics Letters)* **97**, 66002 (2012); I. Kanter *et al.*, *ibid.* **93**, 66001 (2011).
- [6] M. Lakshmanan and D. V. Senthilkumar, *Dynamics of Nonlinear Time-Delay Systems* (Springer, Berlin, 2010).
- [7] W. Just *et al.*, *Phil. Trans. R. Soc. A* **368**, 303 (2010).
- [8] J. D. Farmer, *Physica D* **4**, 366 (1982).
- [9] S. Lepri *et al.*, *Physica D* **70**, 235 (1994).
- [10] G. Giacomelli and A. Politi, *Phys. Rev. Lett.* **76**, 2686 (1996).
- [11] T. Erneux, *Applied Delay Differential Equations* (Springer, New York, 2009).
- [12] E. Klein *et al.*, *Phys. Rev. E* **73**, 066214 (2006).
- [13] I. Fischer *et al.*, *Phys. Rev. Lett.* **97**, 123902 (2006).
- [14] V. Flunkert *et al.*, *Phys. Rev. Lett.* **105**, 254101 (2010).
- [15] A. Argyris *et al.*, *Nature* **438**, 343 (2005).
- [16] I. Kanter *et al.*, *Phys. Rev. Lett.* **101**, 084102 (2008).
- [17] S. Heiligenthal *et al.*, *Phys. Rev. Lett.* **107**, 234102 (2011).
- [18] L. M. Pecora and T. L. Carroll, *Phys. Rev. Lett.* **64**, 821 (1990).
- [19] H. D. I. Abarbanel, N. F. Rulkov, and M. M. Sushchik, *Phys. Rev. E* **53**, 4528 (1996).
- [20] T. Jüngling and W. Kinzel, “Scaling of Lyapunov exponents in chaotic delay systems,” (2012), unpublished.
- [21] U. Parlitz, *NOLTA, IEICE* **3**, 113 (2012).
- [22] M. C. Soriano *et al.*, *Phys. Rev. Lett.* **108**, 134101 (2012).
- [23] A. A. Koronovskii, O. I. Moskalenko, and A. E. Hramov, *Phys. Rev. E* **84**, 037201 (2011).
- [24] T. Schreiber, *Phys. Rev. Lett.* **85**, 461 (2000).
- [25] T. Sano, *Phys. Rev. A* **50**, 2719 (1994).
- [26] J. Mulet and C. R. Mirasso, *Phys. Rev. E* **59**, 5400 (1999).
- [27] M. Lichtner, M. Wolfrum, and S. Yanchuk, *SIAM J. Math. Anal.* **43**, 788 (2011).
- [28] S. Yanchuk and M. Wolfrum, *SIAM J. Appl. Dyn. Syst.* **9**, 519 (2010).
- [29] L. M. Pecora and T. L. Carroll, *Phys. Rev. Lett.* **80**, 2109 (1998).
- [30] T. Heil, I. Fischer, W. Elsässer, J. Mulet, and C. R. Mirasso, *Phys. Rev. Lett.* **86**, 795 (2001).
- [31] V. Ahlers *et al.*, *Phys. Rev. E* **58**, 7208 (1998).